


# A low-order adaptive engine model for SI–HCCI mode transition control applications with cam switching strategies

International J of Engine Research  
2016, Vol. 17(4) 451–468  
© IMechE 2015  
Reprints and permissions:  
sagepub.co.uk/journalsPermissions.nav  
DOI: 10.1177/1468087415585016  
jer.sagepub.com  


Patrick Gorzelic<sup>1</sup>, Prasad Shingne<sup>1</sup>, Jason Martz<sup>1</sup>, Anna Stefanopoulou<sup>1</sup>,  
Jeff Sterniak<sup>2</sup> and Li Jiang<sup>2</sup>

## Abstract

This article presents a low-order engine model to support model-based control development for mode transitions between spark ignition (SI) and homogeneous charge compression ignition (HCCI) combustion modes in gasoline engines. The modeling methodology focuses on cam switching mode transition strategies wherein the mode is abruptly changed between SI and recompression HCCI via a switch of the cam lift and phasing. The model is parameterized to a wide range of steady-state data which are selected to include conditions pertinent to cam switching mode transitions. An additional HCCI combustion model parameter is augmented and tuned based on transient data from SI to HCCI mode transitions where the conditions can be significantly outside any contained in the baseline steady-state parameterization. An adaptation routine is given which allows transient data be assimilated in online operation to update the augmented parameter and improve SI–HCCI transition predictions. With the baseline steady-state parameterization and augmented mode transition parameter, the model is shown to reproduce both steady-state data and transient performance output time histories from SI–HCCI transitions with considerable accuracy.

## Keywords

HCCI control-oriented modeling, HCCI low-order modeling, SI–HCCI mode transition, SI–HCCI mode switch

Date received: 16 November 2014; accepted: 2 April 2015

## Introduction

The fuel economy benefits and low nitrogen oxide emissions of homogeneous charge compression ignition (HCCI) combustion have made it a highly pursued technology to improve upon traditional spark ignition (SI) combustion in gasoline engines.<sup>1</sup> Due to boundaries on the stability and harshness of combustion, HCCI is only feasible over a low to mid speed and load range of conventional gasoline engines.<sup>2</sup> Outside this feasible range, the engine must revert to SI combustion, which necessitates transitions to/from HCCI when the feasible range is entered/exited in online operation. Many studies have approached SI/HCCI mode transitions by means of open-loop experimentation,<sup>3–12</sup> wherein actuator sequences for the mode transition are tuned through trial and error and scheduled in look-up tables based on operating condition. Model-based feedback control methods such as those in Gorzelic et al.<sup>13</sup>

and Ravi et al.<sup>14</sup> may help mitigate the calibration burden associated with scheduling actuator sequences across the entire HCCI feasible range, as well as improve robustness in that the controller can respond based on measurements of the engine condition as opposed to offline optimized maps. This article concerns the development and validation of a model for use in such model-based mode transition control approaches.

<sup>1</sup>Department of Mechanical Engineering, University of Michigan, Ann Arbor, MI, USA

<sup>2</sup>Robert Bosch LLC, Farmington Hills, MI, USA

### Corresponding author:

Patrick Gorzelic, Department of Mechanical Engineering, University of Michigan, Ann Arbor, MI, USA.  
Email: pgoz@umich.edu

Modeling for SI/HCCI mode transitions has been examined in previous works,<sup>15–18</sup> where Roelle et al.<sup>15</sup> and their successors Shaver et al.<sup>16</sup> consider distinct SI and HCCI modes while Yang et al.<sup>17</sup> use a unified model for SI, HCCI, and hybrid combustion between the two modes which is later extended to two zones.<sup>18</sup> The models in these studies are formulated according to the crank angle–based approach, wherein the model states evolve in the crank angle domain and are numerically integrated throughout the cycle to calculate performance outputs such as torque and combustion phasing. This article is concerned with developing a model for mode transition control that has a low-order cycle-to-cycle topology, which is more tractable for model-based control design and implementation than the crank angle–based models. An example application of a model with a low-order cycle-to-cycle structure for combustion mode transition control is given in Gorzelic et al.<sup>13</sup> for the SI component of the SI–HCCI mode transition. The disadvantage of such a low-order approach is increased dependency on empirical parameterization relative to crank angle–based approaches, which arises because of the simplifications necessary to avoid more detailed calculations and resulting reduction in model physicality. To compensate for this fact, the model of this article is augmented with an adaptive parameter which assimilates online data from SI–HCCI mode transitions where HCCI conditions are entered which cannot be reached in nominal HCCI operation on which the model parameterization is based. It should be noted that a reduced-order model<sup>19</sup> has been applied for fuel injection timing control in SI–HCCI mode transitions,<sup>14</sup> where it was used in a linearized feedforward calculation. However, the mode transition strategy for which the model<sup>14</sup> was used differed from those considered in this study in that the cams were gradually phased to change the mode from SI to HCCI, while this study assumes an abrupt mode change that is coupled with a switch of the cam lift and phasing. This abrupt mode switch results in a more drastic step in the operating condition when switching from SI to HCCI, which is a major consideration of the modeling methodology of this article.

The article first gives an overview of the baseline mean value engine model (MVEM) for SI and HCCI combustion and presents its parameterization to steady-state data. The steady-state parameterization is structured to accommodate throttled operation and a wide range of air–fuel ratio (AFR) variation, which may be encountered in cam switching mode transition strategies that utilize two-stage cam hardware.<sup>6–11</sup> In these strategies, a set of high-lift/low-lift cams is switched between to enable SI/HCCI operation, respectively. With the use of two-stage cam hardware, it becomes impractical to fully de-throttle the SI combustion at constant load to switch to/from HCCI, in contrast to the case where a more costly variable valve actuation device is used which can be used to control

the cylinder breathing with a fully open throttle.<sup>3–5,16</sup> After presenting the baseline model, a transient simulation against SI–HCCI mode transition data is considered which motivates the introduction of an augmented parameter to improve predictions during SI–HCCI mode transitions. Transient data for the HCCI–SI direction are not examined, leaving the validation and potential modification of the model in this scenario for future work. Following its introduction, a method to adapt the augmented mode transition parameter using online SI–HCCI transition data is given. The model is then tested against multiple experimental SI–HCCI mode transition cases which encompass both varying initial conditions for the HCCI entry point and varying load conditions throughout the transition. The article then concludes with a summary of the important model aspects.

## Mean Value Engine Model

### Model overview

The engine model of this work follows the mean value approach, with discrete cycle-to-cycle combustion models for both SI and HCCI combustion modes that are embedded into a continuous air–path model which is based on zero-dimensional (0-D) manifold filling dynamics. Constant engine speed is assumed and the combustion is constrained to execute on time intervals equivalent to the engine cycle duration. The cycle division of the combustion model is drawn after the blowdown event at exhaust valve opening (EVO), and the coupling between cycles through the recycled exhaust gas is modeled by carrying the temperature and composition of the exhaust gas from one cycle to the next. The cycle-to-cycle coupling variables take the place of discrete time states for the combustion model and are chosen to be the blowdown temperature  $T_{bd}$ , burned gas fraction after combustion  $b_{bd}$ , and unburnt fuel mass fraction after combustion  $f_{bd}$

$$T_{bd} : = T_{cyl} \Big|_{EVO^+} \quad (1)$$

$$b_{bd} : = \frac{m_b}{m_c} \Big|_{EVO^+} \quad (2)$$

$$f_{bd} : = \frac{m_{uf}}{m_c} \Big|_{EVO^+} \quad (3)$$

where  $m_b$  denotes the mass of complete combustion products,  $m_c$  denotes the total cylinder charge,  $m_{uf}$  denotes the mass of unburnt fuel from main combustion, and  $EVO^+$  indicates immediately after EVO. Note that the model's composition calculations lump the cylinder mass into three categories, being fuel, air, and combustion products.

A schematic diagram showing how the combustion model states are used to preserve cycle-to-cycle couplings in an SI–HCCI mode transition scenario is depicted in Figure 1. The SI combustion model

executes on the final SI cycle  $k - 1$  and the exhaust states generated by the SI combustion model at blow-down are stored with a discrete cycle delay (indicated by  $z^{-1}$ ) and used to drive the HCCI combustion model on the next cycle  $k$ . The valve profiles (shown dashed) shift from high lift which typically has positive valve overlap (PVO) to low lift with negative valve overlap (NVO) between the final SI and first HCCI cycles to induce an early exhaust valve closing (EVC) timing and late intake valve opening (IVO) which traps more residuals to promote auto-ignition. The combustion states are used to capture cycle-to-cycle couplings within nominal HCCI operation as well, since in HCCI the cycle-to-cycle coupling is significant due to the high amount of recycled exhaust gas. However, in nominal SI operation where the cycle-to-cycle coupling is mild, it is ignored and the combustion states are calculated only to be passed to the HCCI model in the event of a mode transition.

A brief description of the SI and HCCI combustion models is given below, with a model equation listing being available in Appendix 1. The SI and HCCI models are structurally similar in that both employ polytropic compression and expansion processes with a constant volume heat release, along with regressions for residual gas, air charge, and combustion phasing. Only the form of the regressions changes between the models to represent different physical processes. For this reason, Appendix 1 gives an equation listing only for the HCCI model and omits the SI model. The air-path model is not reviewed because it comes from previous works<sup>20–22</sup> and its main constituents consist of 0-D manifold filling dynamics, which are well known, see, for example, Eriksson.<sup>23</sup> The air-path of the experimental engine for the current model as well as those on which it is based<sup>20–22</sup> does contain a turbocharger; however, experimental data and simulation indicate

that the turbocharger dynamics are negligible at the low loads considered for SI–HCCI mode transitions and can be omitted. While the model description has here been kept brief due to space constraints, a thorough explanation of the model can be found elsewhere.<sup>24</sup>

The HCCI model of this article builds on previous recompression HCCI modeling work in Jade et al.,<sup>25</sup> introducing new compositional dependencies to capture a wider range of operating conditions and an alternate cylinder breathing model which proved favorable for extension to SI–HCCI transitions. The effects of AFR and temperature during the recompression period on chemical reactions which can go on to affect the fuel ignition delay are incorporated into the Arrhenius threshold for start of combustion (see equation (28)). The use of the Arrhenius threshold to model these effects follows the logic of Ravi et al.<sup>26</sup> The form of these dependencies is based on the observations of Song and Edwards.<sup>27</sup> This study found that shortest ignition delays were obtained at intermediate AFRs, where a balance was struck between pyrolysis reactions that enhance ignitability and reformation and exothermic reactions that inhibit ignitability. Without these dependencies, fits to combustion phasing data were poor even when multiple correlations from the literature<sup>19,28–30</sup> were tried.

Recompression heat release (RCHR) of recycled unburnt fuel from main combustion was apparent in SI–HCCI mode transition data as will later be seen, and so is included via relationships modified after Hellström and Stefanopoulou.<sup>31</sup> The late phasing combustion efficiency is extended to contain a dependency on fuel mass  $m_f$  to capture changes in the late phasing stability limit with load. The RCHR model is simplified from that in Hellström and Stefanopoulou<sup>31</sup> in that instantaneous heat release of unburnt fuel during

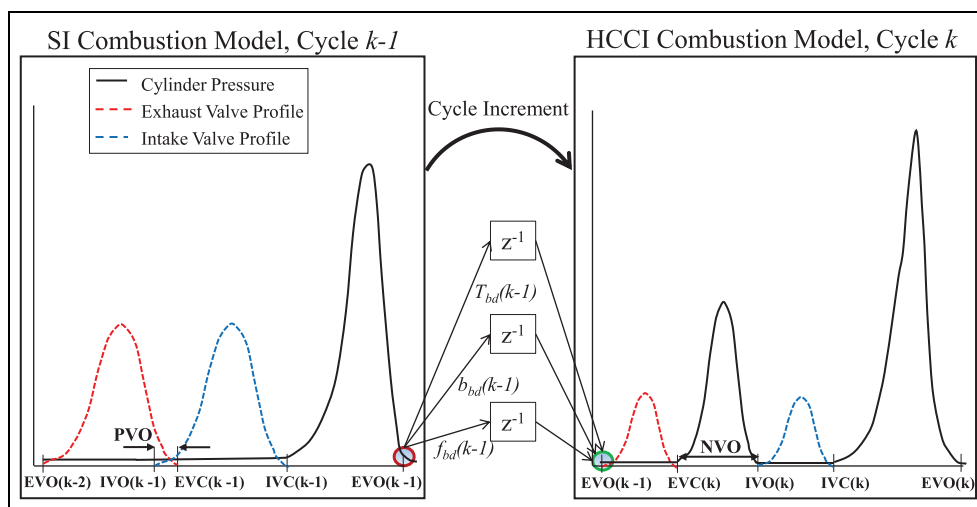


**Figure 1.** Diagram of combustion model cycle division showing how exhaust gas states link SI and HCCI combustion models during a SI–HCCI switch.  $z^{-1}$  indicates a discrete unit (cycle) delay.

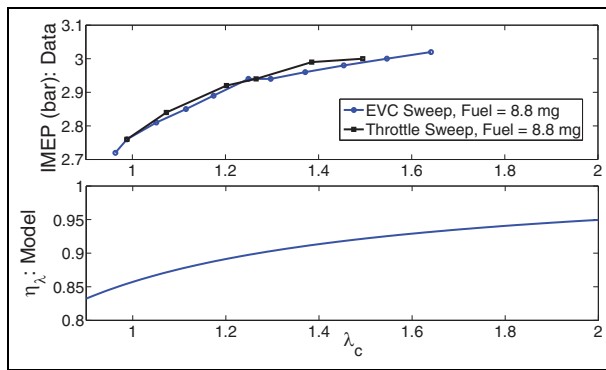


**Figure 2.** Top: IMEP measurements in steady-state actuator sweeps with high AFR variation; bottom: profile of model combined thermal and combustion efficiency as a function of  $\lambda_c$ .

recompression is taken to occur with 100% efficiency directly at EVC. The heat release was chosen to be at EVC because this conforms with the rest of model structure and aids the model regression. Other details of the HCCI model can be found in Appendix 1.

A combined thermal and combustion efficiency term  $\eta_{\lambda}$  (see equation (37)) is introduced as a function of the in-cylinder relative AFR  $\lambda_c$  to account for changes in work output as AFR is varied by adjusting the temperature and hence pressure rise due to combustion. These changes in work output associated with varying AFR are exemplified in the constant fuel actuator sweeps in Figure 2. The  $\eta_{\lambda}$  term represents mainly the effects of combustion efficiency as  $\lambda_c$  nears stoichiometry and more the effect of thermal efficiency as  $\lambda_c$  becomes significantly lean.

The SI combustion model follows the same structure as the HCCI model, but with different regressions for in-cylinder residual, air charge, and combustion phasing. The regressions for these quantities take the form of polynomial basis functions in terms of key variables such as the intake pressure, valve timings, fuel quantity, and spark timing. The regression for cylinder air flow follows the form in Lee et al.<sup>21</sup> and Jankovic and Magner.<sup>32</sup> Combustion efficiency for the model's constant volume heat release is set to unity, and the crank angle of combustion is defined following the logic in Eriksson and Andersson,<sup>33</sup> where the 50% burn angle  $\theta_{50}$  for maximum brake torque is taken at  $7^\circ$  after top dead center (aTDC) for SI combustion.

In parameterization of the combustion models, a simple approach is used for the SI model where each of the model's regressions is fit individually to match its respective measured/post-processed data values. This suffices because cycle-to-cycle couplings are ignored, and hence the model predictions on any given cycle are independent of the predictions on all other cycles. However, for the HCCI model, the inherent cycle-to-cycle feedback induced by the recycled exhaust temperature and composition states of the model can result in large prediction errors from compounding of

modeling error over many cycles, even if the individual regressions are satisfactory. To cope with this issue, the HCCI model parameters are regressed in an iterative routine wherein the exhaust gas states are recycled between subsequent iterations until the state values converge. A description of the iterative parameterization routine is given in Appendix 2.

### Steady-state fitting results

The test engine for this work is a 2-L, four-cylinder engine with a geometric compression ratio of 11.7:1. The model is parameterized to a single cylinder of the four. Dual SI/HCCI operation is enabled by a two-stage cam system with a set of high-lift cams for SI operation and low-lift cams for recompression HCCI operation, similar to the studies of Tian et al.,<sup>7</sup> Cairns and Blaxill,<sup>8</sup> Kalian et al.,<sup>9</sup> Wu et al.,<sup>10</sup> and Nier et al.<sup>11</sup> The valve timings for the high-lift and low-lift cams are offset by a fixed crank angle amount so that when the cams switch, the valve timings instantaneously shift. This offset is characterized by the difference between the EVC and IVO timings between the cam sets, which are equal to  $-34^\circ$  and  $47^\circ$ , respectively. The high and low cam lifts/durations are fixed at 10 mm/ $225^\circ$  and 4 mm/ $114^\circ$ , respectively, and the valve timings are controlled with electronic cam phasers.

**HCCI model fit results.** The dataset used to parameterize the HCCI model consists of a 526-point grid of actuator sweeps at a single engine speed of 2000 r/min with the outermost swept variable being fuel mass, followed by intake manifold pressure (adjusted via throttle) and then EVC timing, and the innermost variable being injection timing. Several direct throttle and EVC sweeps were also carried out to clearly discern the trend in the outputs with respect to these variables. Intake valve timing was held fixed with intake valve closing (IVC) near bottom dead center (BDC), as it was observed to have only a small effect on combustion when maintained in the vicinity of BDC. The grid of inputs and the corresponding performance outputs of  $\theta_{50}$ , net mean effective pressure (NMEP), and  $\lambda$  are shown in Figure 3. The model parameters are regressed using the algorithm given in Appendix 2, and the reproduction of the performance outputs is plotted against the data. As can be seen, the model reproduces the performance outputs with good accuracy for a low-order model considering the wide range of actuator settings over which it is fit. A summary of the swept input and output range and mean and maximum absolute errors is given in Table 1.

The bottom subplot of Figure 3 shows that for much of the parameterized range, the model's prediction of unburnt fuel mass  $m_{uf}$  follows the same trend as the combustion phasing standard deviation  $\sigma(\theta_{50})$ . This is consistent with the logic in Hellström et al.,<sup>34</sup> which explains that unburnt fuel from incomplete burns at late combustion phasing can create a cycle-to-cycle

**Table 1.** Swept range of inputs and outputs in HCCI model parameterization data.

	Minimum	Maximum	Mean Abs. Error	Maximum Abs. Error
$\theta_{soi}$ (bTDC)	300	390	–	–
$\theta_{evc}$ (aTDC)	248	283	–	–
$p_{im}$ (bar)	0.85	1	–	–
$m_f$ (mg)	7.2	10.5	–	–
$\theta_{50}$ (aTDC)	–2	11	0.86°	5.16°
NMEP (bar)	1.7	3	2.06%	12.2%
$\lambda$	0.92	1.5	2.81%	11.2%

AE: absolute error; bTDC: before top dead center; aTDC: after top dead center; NMEP: net mean effective pressure; CAD: crank angle degree. Mean and maximum absolute errors between model and measurement listed for outputs.  $\theta_{50}$  error reported in CAD to avoid division by small numbers at  $\theta_{50}$  near TDC.

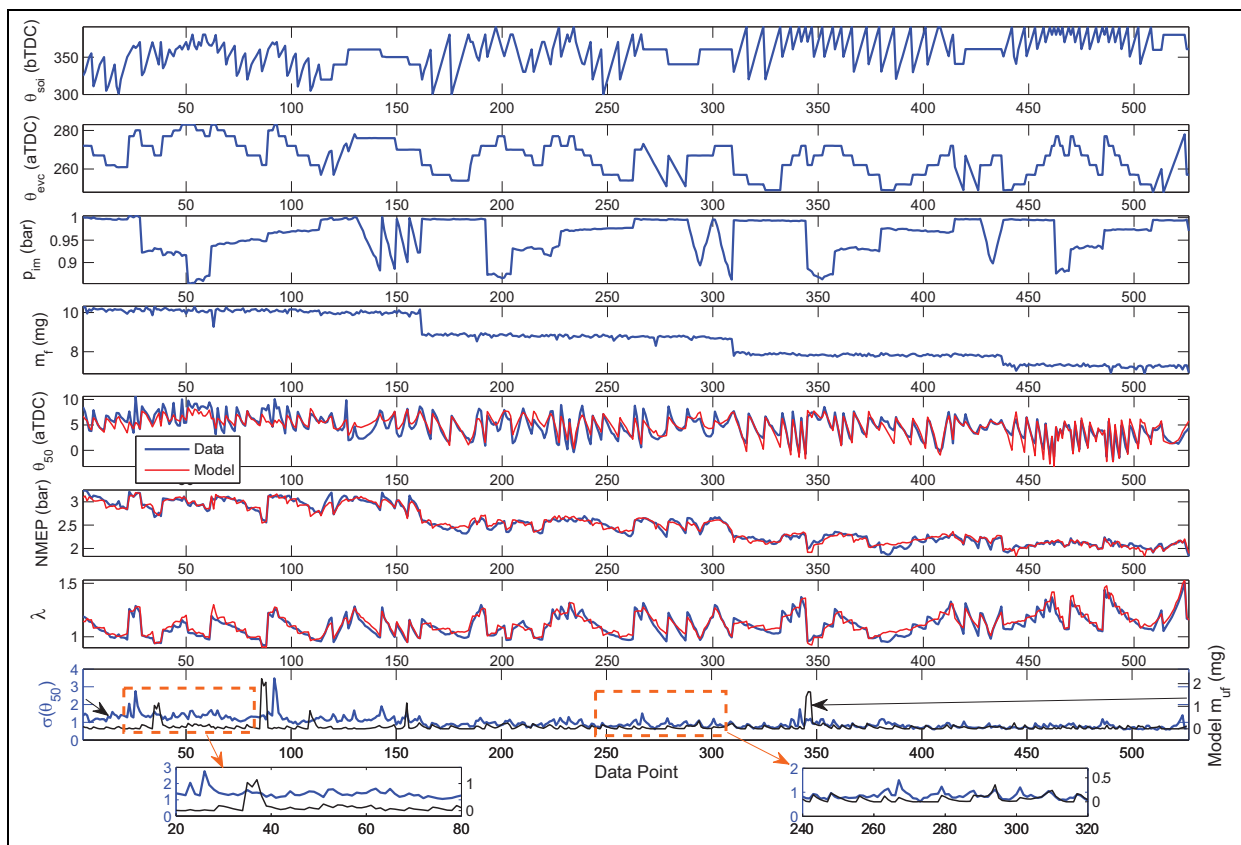


**Figure 3.** Input grid and modeled versus measured outputs for steady-state HCCI model parameterization data. Bottom subplot is shown with close-ups so that the  $\theta_{50}$  standard deviation  $\sigma(\theta_{50})$  can be compared to the model's mass of unburnt fuel calculation  $m_{uf}$  more clearly.

coupling which leads to oscillatory behavior and hence higher standard deviation in the combustion phasing. There are some regions where the model's  $m_{uf}$  prediction does not follow  $\sigma(\theta_{50})$  as exemplified in the left-hand close-up plot between points 20 and 80, at which points the model's  $\theta_{50}$  fit can be observed to underpredict some of the late phasing conditions which give rise to unburnt fuel. This  $\theta_{50}$  error may be influenced by the high sensitivity of the model's Arrhenius correlation for combustion phasing at very late, near-misfire conditions, which makes small modeling errors have a large effect. The model's trends in  $m_{uf}$  versus  $\sigma(\theta_{50})$  may also be enhanced if the model is conditioned on long

duration cycle-to-cycle high cyclic variability data as in Hellström and Stefanopoulou,<sup>31</sup> which was not available for this study.

To test the ability of the model to extrapolate, the model parameterization was repeated on a subset of the data which excludes all points at the lowest load in the dataset, or the last 89 points in Figure 3. These excluded points encompass not only a different load from the rest of the data but also different  $p_{im}/\theta_{evc}/\theta_{soi}$  input combinations and leaner mixtures. When evaluated on the excluded points, the model maintained correct trends and produced mean absolute errors of 1.4 crank angle degrees (CAD), 2.1%, and 4.5% for  $\theta_{50}$ ,

**Table 2.** Swept range of inputs and outputs in SI model parameterization data.

	Minimum	Maximum	Mean Abs. Error	Maximum Abs. Error
$\theta_{sp}$ (aTDC)	-33	-6	-	-
$m_f$ (mg)	8.19	15.95	-	-
$\theta_{ivo}$ (aTDC)	344	370	-	-
$\theta_{evc}$ (aTDC)	297	370	-	-
$\theta_{50}$ (aTDC)	0.4	34.2	0.89°	4.38°
$NMEP$ (bar)	1.7	3.95	2.43%	9.13%
$m_a$ (mg)	120	226	1.57%	6.44%

AE: absolute error; aTDC: after top dead center;  $NMEP$ : net mean effective pressure; CAD: crank angle degree.

Mean and maximum absolute errors between model and measurement listed for outputs.  $\theta_{50}$  error reported in CAD to avoid division by small numbers at  $\theta_{50}$  near TDC.

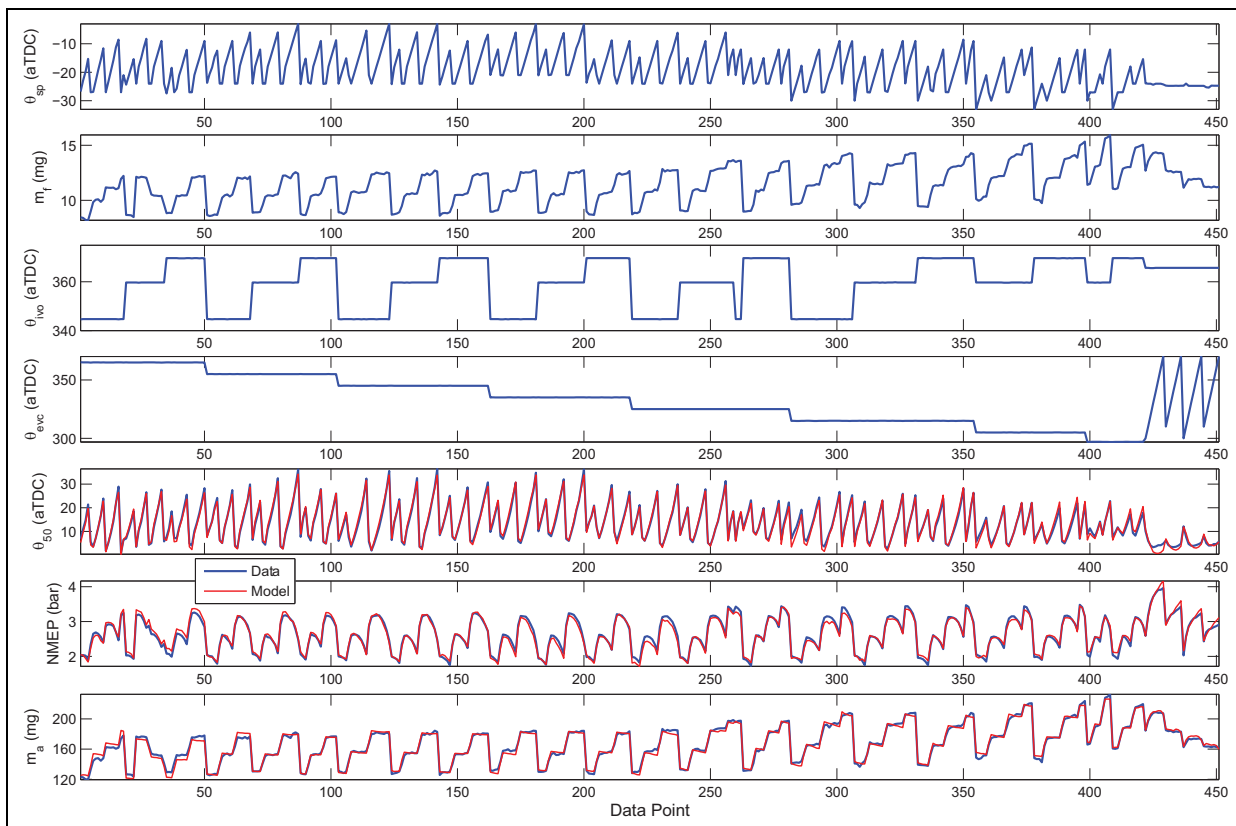


**Figure 4.** Input grid and modeled versus measured outputs for steady-state SI model parameterization data. Mass of air  $m_a$  is shown in place of  $\lambda$  as in Figure 3 because stoichiometry was maintained throughout the sweeps.

$NMEP$ , and  $\lambda$ , respectively, which are higher than in Table 1 but acceptable for extrapolation.

**SI model fit results.** For the SI model parameterization sweeps, AFR was held fixed at stoichiometry and the fuel and air were varied simultaneously through adjusting the throttle. Engine speed was also constant at 2000 r/min. The innermost variable of the input grid was spark timing  $\theta_{sp}$ , followed by fuel (and hence air), then the intake valve timing, and finally exhaust valve timing. The exhaust valve timing was swept to very advanced positions, as the mode transition strategy involves advancing the EVC timing while in SI mode to trap more residual and assist in increasing intake pressure at constant load. The 451-point input grid and

modeled versus measured outputs of  $\theta_{50}$ ,  $NMEP$ , and air mass  $m_a$  are shown in Figure 4, and the summary fit statistics are given in Table 2. Air mass is shown as opposed to  $\lambda$  because AFR is held fixed. Like the HCCI model, the SI model fits the steady-state parameterization data with good accuracy.

### Augmented parameter for SI-HCCI transitions

This section draws on previous work<sup>35</sup> and discusses results from an experimental open-loop SI-HCCI mode transition which motivate the introduction of an augmented residual gas correction parameter on the initial cycle when HCCI is entered.



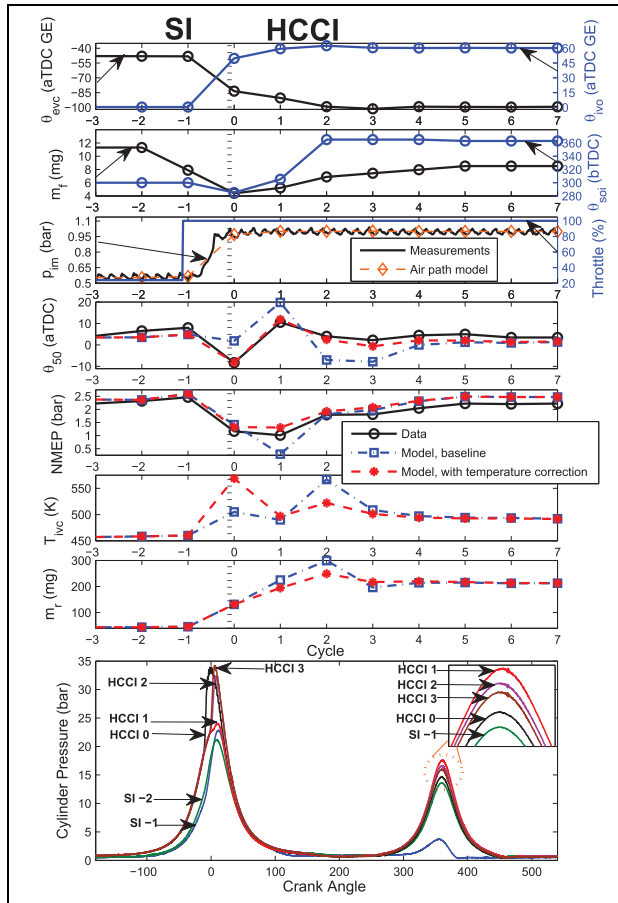


**Figure 5.** Cycle-by-cycle inputs and outputs and crank angle-resolved in-cylinder pressure during open-loop SI–HCCI mode transition. *SI – 1* indicates the final SI cycle and *HCCI 0* indicates the first HCCI cycle. Model reproduction of outputs with and without the introduced residual temperature correction is shown.

### Mode transition overview

The format for the mode transition experiments was to drive the engine to a steady-state condition in SI mode which was appropriate for switching to HCCI, and then to switch the intake and exhaust cams simultaneously. The cams switch from high to low lift during the closed-valve portion of the final SI cycle so that at the EVO event of the final SI cycle, the low-lift cams are in place. The SI switch point condition was set with an advanced exhaust cam phasing and retarded intake cam phasing to promote higher intake manifold pressure and further throttle opening while maintaining constant load and AFR before switching to HCCI. The retarded intake phasing reduces cylinder air charge through late IVC timing, and the advanced exhaust phasing reduces cylinder air charge by trapping more residual mass with early EVC. The early EVC also leads to early EVO which reduces the work output by reducing the length of the expansion stroke, hence requiring a greater throttle opening to maintain the load. The throttle was commanded wide open roughly

20–30 ms before the first low-lift breathing event. The spark timing is placed 20° aTDC when HCCI engages to prevent interaction with the combustion. To simulate the mode transition, the measured throttle position is input to the air-path model on a time-sampled basis, and the measured cam phaser positions and commanded fuel quantity, injection timing, and spark timing are input to the combustion model on a cycle-by-cycle basis.

The combustion response and the corresponding input sequences for an SI–HCCI mode transition trial are shown in Figure 5, where *SI – 1* and *HCCI 0* designate the final SI cycle and first HCCI cycle, respectively, following the notation in Shaver et al.<sup>16</sup> The independent axis of the time-based measurements of intake manifold pressure and throttle command is transformed in order to plot these variables against the engine cycle. The cams switch during the closed-valve portion of cycle *SI – 1* which causes a sudden increase in the recompression pressure and jump in the valve timings  $\theta_{evc}$  and  $\theta_{ivo}$ . In anticipation of the high exhaust temperature that is carried over from the final SI cycle, both the  $\theta_{evc}$  and  $\theta_{soi}$  timings are placed much later than their steady-state set points when HCCI is entered to retard combustion phasing. However, on cycle *HCCI 0*, the combustion phasing is still early, accompanied by a high pressure rise rate. The combustion phasing then shifts later on cycle *HCCI 1* where the exhaust temperature is now lower as a result of HCCI combustion. This initially early and then late combustion phasing caused by the cycle-to-cycle temperature coupling is the same phenomenon observed in the mode transition portrayed in Shaver et al.<sup>16</sup> Following the late combustion phasing and weak heat release on the cycle *HCCI 1*, the recompression event exhibits an enlarged peak pressure which occurs significantly aTDC, which indicates RCHR of unburnt fuel from the main combustion event. This RCHR in conjunction with the earlier injection timing causes the combustion phasing to advance on cycle *HCCI 2*, and from here the transient becomes milder and the combustion settles to steady state.

As is apparent from the dash-square  $\theta_{50}$  response in Figure 5, the baseline model does not capture the extremely advanced combustion phasing on cycle *HCCI 0* in the data, despite that it is equipped with exhaust temperature dynamics and fits a large steady-state dataset with good accuracy (see Figure 3). Significant phasing and torque errors follow the next few transient cycles as well, which are influenced by the large initial error as will be seen. The plot of the predicted in-cylinder temperature at IVC,  $T_{ive}$ , shows that the baseline model predicts a  $T_{ive}$  value on cycle *HCCI 0* which is similar to the value at cycles *HCCI 6* and *HCCI 7* toward the end of the transition. Due to the higher exhaust temperature of SI combustion that is carried over into cycle *HCCI 0*, the  $T_{ive}$  on this first

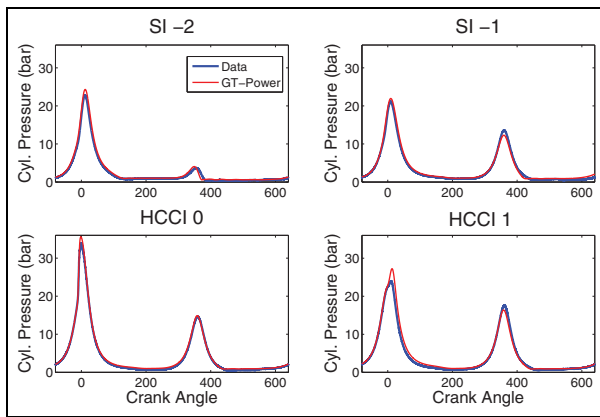


**Figure 6.** Comparison of experimental versus GT-Power simulation in-cylinder pressure during an SI-HCCI mode transition.

HCCI cycle may be expected to be higher than the cycles toward the end of the transition where the residual temperature falls closer to nominal HCCI levels. If the model's  $T_{ivc}$  is underpredicted on cycle *HCCI 0*, it could be responsible for the erroneous  $\theta_{50}$  prediction. However, a competing effect is that the residual mass  $m_r$  is very low on cycle *HCCI 0* due to the very late  $\theta_{evc}$  timing as well as low exhaust gas density from the higher exhaust temperature, which should act to reduce  $T_{ivc}$ . The uncertainty in the model's in-cylinder temperature prediction on cycle *HCCI 0* warrants further investigation with higher fidelity modeling tools.

#### Mode transition predictions using crank angle-based model

A simplified single-cylinder GT-Power simulation was carried out to aid in drawing conclusions about the baseline model's combustion phasing error on cycle *HCCI 0*. The GT-Power simulation is not intended to reproduce absolute values from the experiment, but rather to gain a better understanding of the unmeasured variables during the transient phase of the SI-HCCI mode transition, such as the in-cylinder temperature. The measured intake and exhaust manifold pressures and temperatures were specified as intake and exhaust runner boundary conditions on a crank angle basis, and the valve profiles/timings from the experiment were imposed to capture the effect of the cam switch from high to low lift and rapid cam phasing. The combustion portion of each cycle is specified by imposing measured burn angles and Wiebe function parameters on a cycle-by-cycle basis, and the remainder of the cycle is generated through a crank angle-based engine model and one-dimensional gas dynamics calculations. To validate the GT-Power simulation, experimental pressure traces are compared versus those generated by the simulation in Figure 6. The adequate agreement between GT-Power and experiment suggests reasonable GT-Power model prediction accuracy.

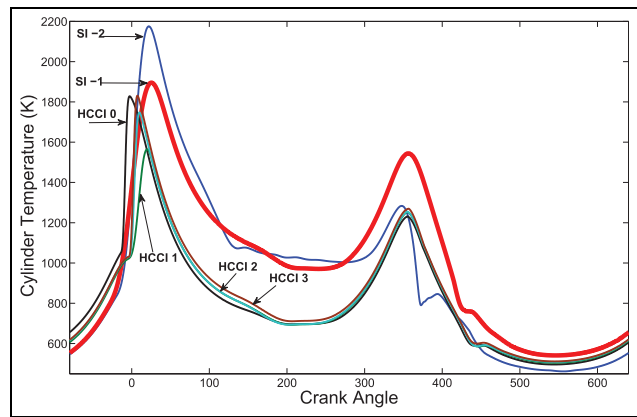


**Figure 7.** In-cylinder temperature traces generated by GT-Power SI-HCCI mode transition simulation. The final SI cycle whose recompression event yields an extremely high temperature leading to the first HCCI cycle is highlighted.

Figure 7 plots consecutive in-cylinder temperature traces calculated by GT-Power during the mode switch from SI to HCCI. The switch of the cams from high to low lift is marked by a shift from an earlier blowdown process and milder recompression peak on cycle *SI -2* to a larger approximately symmetric recompression peak on cycle *SI -1*. The sudden temperature drop near TDC of recompression on *SI -2* is due to an earlier IVO from the high-lift intake cam, which is followed by a reversion process of the in-cylinder residual that is ejected into the intake manifold. Comparing the recompression period on cycle *SI -1* leading into *HCCI 0* to the remainder of the HCCI cycles, there is a clear trend that the temperature at the end of recompression is roughly 200 K higher than the others, which goes onto yield a significantly higher temperature after the intake event. This suggests that the baseline model does indeed underpredict in-cylinder temperature on cycle *HCCI 0* in Figure 5, as its  $T_{ivc}$  shows only minor differences from the later HCCI cycles.

In tracing the source of model error on cycle *HCCI 0*, it can be noted that the exceedingly high recompression temperature leading into cycle *HCCI 0* only occurs during SI-HCCI switch transients when the high-temperature SI exhaust undergoes recompression with the low-lift cams. It is thus uncertain how the low-order model will extrapolate to such a condition as it is outside the nominal steady-state HCCI parameterized range. The competing effect of low residual mass noted previously further complicates this extrapolation. Several other transient effects, which occur only during SI-HCCI transitions, may also be influencing the model error, such as amplified manifold dynamics due to the rapid dethrottling and increased intake temperature due to higher fluid velocities. However, for the simplified low-order modeling approach, the prediction error is lumped into the excursion of the residual temperature from nominal HCCI conditions, as this is an effect that clearly introduces model uncertainty.



### Residual gas temperature correction for initial HCCI cycle

Based on the observations from the preceding subsections, the model's prediction error when entering HCCI is attributed solely to the high residual temperature that is carried over from SI. To maintain low model order, the model error on cycle  $HCCI 0$  is accounted for with an empirical correction factor which parameterizes the model error into the residual temperature. The correction factor is placed on the model's residual gas temperature calculation  $T_r$  that appears in the energy balance type regression for the mass of inducted air (see Appendix 1 for more information on this regression), which is applied only on the first HCCI cycle

$$m_a^{in} = \begin{cases} \frac{1}{T_{im}} \left[ a_1 p_{ivc} V_{ivc} - (m_r + m_f^{in})(k_r T_r) + a_2 \right], & HCCI 0 \\ \frac{1}{T_{im}} \left[ a_1 p_{ivc} V_{ivc} - (m_r + m_f^{in}) T_r + a_2 \right], & \text{else} \end{cases} \quad (4)$$

where  $k_r > 0$  is the residual gas correction factor;  $T_{im}$  is the intake manifold temperature;  $p_{ivc}$  and  $V_{ivc}$  are the pressure and volume at IVC, respectively;  $a_1$  and  $a_2$  are fitting coefficients; and  $HCCI 0$  indicates the first cycle when switching to HCCI. In parameterization,  $k_r$  is regressed to match combustion phasing during the transient HCCI phase of the SI–HCCI transition. The reason for this choice is that  $k_r$  is coupled to the combustion phasing through the in-cylinder temperature and that the combustion phasing is directly measurable during the transient SI–HCCI phase which makes it convenient for implementation. For the mode transition of Figure 5,  $k_r = 1.14$ .

With the augmented residual temperature correction, the  $T_{ivc}$  predicted by the model on cycle  $HCCI 0$  in Figure 5 is increased relative to its steady-state value, following the trend observed in the GT-Power simulation. Comparison of the model's  $T_r$  prediction with the temperature at IVO  $T_{ivo}$  produced by GT-Power suggested that the trend in residual temperature also matches the GT-Power simulation more closely when the residual temperature correction is applied, taking  $T_{ivo}$  as indicative of residual temperature in GT-Power. Comparing on a percentage basis to omit steady-state offsets between the model and GT-Power predictions, the model's  $T_r$  calculation on cycle  $HCCI 0$  was elevated by 37% relative to its steady-state value with the residual temperature correction active as opposed to only 14% without the correction, while the  $T_{ivo}$  in GT-Power was elevated by 33% relative to its steady-state value on cycle  $HCCI 0$ . Figure 5 also shows that the  $\theta_{50}$  response predicted by the model now matches the data well not only on cycle  $HCCI 0$  where the correction is active but for the entire transient process. This indicates that the main effect driving the erroneous transient response predicted by the nominal model is

the error induced by the extreme conditions on the cycle  $HCCI 0$ , which goes on to affect subsequent cycles through the cycle-to-cycle states. Once this error is corrected for, the nominal model can capture the remainder of the transient response, as the conditions become much closer to nominal HCCI.

### Adaptive tuning of augmented parameter

#### Motivation and description of adaptive tuning method

An important consideration from a control design standpoint for SI–HCCI transitions is that on the first HCCI cycle of the transition, no HCCI combustion feedback is yet available, and so a model-based controller must rely completely on the model predictions. The only way to incorporate feedback to rectify the controller response on this first HCCI cycle is thus to assimilate transient data after the fact, to improve the model predictions for the next mode transition. It has also been discussed that the conditions on the first HCCI cycle tend to be outside the steady-state HCCI operating regime used to parameterize the model, and so using online data to improve the model predictions when such conditions are entered can help alleviate any shortcomings of the model in extrapolating to these conditions. The mode transition corrective parameter  $k_r$  serves as an ideal candidate for such an online model update, as it is specifically introduced to improve the model predictions on the first HCCI switching cycle and is tuned exclusively to transient SI–HCCI mode transition data. Adjusting  $k_r$  may yield performance benefits for the transient cycles following the initial HCCI cycle as well, as the degree of model error on the first HCCI cycle has been shown to have a significant impact on the following cycles through the dynamic cycle-to-cycle coupling.

To develop an online parameter update method for  $k_r$ , a simplified approach is taken where  $k_r$  is adjusted to match combustion phasing on the first and only the first HCCI cycle of the SI–HCCI transition. This method neglects how the choice of  $k_r$  affects cycles after the first HCCI cycle through the thermal and compositional coupling, and so may yield suboptimal predictions for the overall transient response. However, limiting attention to the first HCCI cycle yields a far more tractable algorithm and can still give significant improvements in model accuracy during the mode transition as will be shown.

The high-level method for the  $k_r$  parameter update is to back-track through the model to solve for the  $k_r$  value that yields a perfect match of  $\theta_{50}$  on the first HCCI cycle of the transition so that a linear update law can be used. The algorithm starts with the measured  $\theta_{50}$  on the first HCCI cycle  $\theta_{50}^{meas}$ , which is used with equation (31) to solve for the corresponding start of combustion  $\theta_{soc}^*$

$$\theta_{soc}^* = \frac{1}{a_1} (\theta_{50}^{meas} - a_0) \Big|_{HCCI0} \quad (5)$$

where the coefficients  $a_1$  and  $a_0$  come from equation (31) and  $|_{HCCI0}$  indicates a quantity evaluated on the first HCCI cycle. Since  $k_r$  affects  $\theta_{soc}$  through the in-cylinder temperature, it must ultimately be back-solved from the Arrhenius integral (27), which requires a numerical inversion. Toward this end, a simple Newton–Raphson inversion is applied, where the independent variable is taken as the temperature at IVC which imposes  $\theta_{soc} = \theta_{soc}^*$ , denoted by  $T_{ivc}^*$ . The Jacobian of the Newton–Raphson algorithm is formed using a simple forward difference approximation to minimize complexity. Simulations show that  $T_{ivc}^*$  converges within 1 K in two to four iterations, which necessitates four to eight evaluations of the Arrhenius integral in equation (27). This may be computationally feasible in real-time on slower sampling loops (e.g. 100 ms); however, if computation time proves to be a problem, then the parameter update can run as an event-triggered background task, as it only needs to execute once for each new mode transition. Computation time can also be drastically reduced by storage of the Arrhenius integral in a look-up table. When  $T_{ivc}^*$  is found, it can be combined with equations (4), (22), and (24) to solve for the target correction  $k_r^*$ ,

$$k_r^* = \frac{p_{ivc} V_{ivc} \left( a_1 - \frac{T_{im}}{R T_{ivc}^*} \right) + (m_r + m_f) T_{im} + a_2}{(m_r + m_f) T_r} \Big|_{HCCI0} \quad (6)$$

where the coefficients  $a_1$  and  $a_2$  come from equation (4).

In the general case where mode transitions must take place at varying operating conditions throughout a drive cycle,<sup>36</sup>  $k_r^*$  will most likely vary with engine operating variables such as speed and load, as well as with time as the engine behavior drifts over the life-cycle of the engine. To capture this variation, it is advisable to parameterize  $k_r$  as a function of operating condition and update the parameterization with each new mode transition measurement using a recursive parameter update method. This is in contrast to simply resetting the value of  $k_r$  equal to the solution of equation (6) after each new mode transition, which will not capture any operating condition dependency and will increase susceptibility to noise and disturbances by discarding older data. A simple linear parameterization for  $k_r$  based on EVC timing is later employed to capture an SI–HCCI transition dataset that extends to multiple operating conditions. For simplicity of illustration, the example adaptive tuning simulations in this section consider the case where  $k_r$  is adapted to account for drifts and parameter errors over time at a single operating condition. In this case, the operating condition dependency of  $k_r^*$  is unnecessary, and so the estimate of  $k_r^*$  takes the form of a single parameter  $\hat{k}_r$  with only a time dependence

$$k_r^* \approx \hat{k}_r(m) \quad (7)$$

where  $m$  is the iteration index which increments at each successive mode transition and so represents an event-based time dependence.

To facilitate real-time implementation of the proposed adaptation, it is desirable to use a linear parameter update law to tune the  $k_r$  value, which is applicable under the condition that the parameterization of  $k_r$  is linear in the fitting coefficients. Several linear parameter update laws exist, such as the recursive least squares and simplified the projection (gradient) algorithms, along with the stochastic counterpart to the projection algorithm, the stochastic approximation algorithm.<sup>37</sup> All these algorithms follow a parameter update law of the form

$$\hat{k}_r(m) = \hat{k}_r(m-1) + G(m) \left( k_r^*(m) - \hat{k}_r(m-1) \right) \quad (8)$$

where the selection of the adaptive gain  $G(m)$  is the main differentiating factor among the algorithms. In general, the recursive least squares algorithm is preferable to use when possible, for its faster convergence and bounded parameter variance properties as compared to the simplified algorithms. However, the recursive least squares algorithm is more computationally demanding than the others so that if the number of parameters becomes high, it may be prudent to use one of the simplified algorithms. For the basic example cases considered where only one parameter ( $\hat{k}_r$ ) is being estimated as a function of time, it can be shown that each algorithm's expression for  $G(m)$  reduces to a constant so that all algorithms are equivalent and  $G(m) \equiv G$  becomes a constant tuning factor. Parameter adaptation results are thus representative of all the mentioned algorithms. When more parameters are included in the  $k_r$  expression to capture dependency on operating condition, the value of  $G(m)$  must be calculated for each new data point following the formula for the chosen algorithm, all of which can be found in, for example, Astrom and Wittenmark.<sup>37</sup> The parameter update method is summarized in the block diagram Figure 8, where intermediate model variables necessary to carry out the update have been shown with a superscript *mod* and must be evaluated with equations (11)–(20).

### Adaptive tuning simulations

To demonstrate the effect of the  $k_r$  adaptation, a simple example is given wherein the estimate  $\hat{k}_r$  is initialized with an error of 0.1 from the nominal value for the mode transition sequence in Figure 5 and adapted to consecutive trials of the same mode transition sequence. For simplicity, only the HCCI phase of the mode transition is simulated on each iteration of the mode transition sequence because the SI model predictions are exactly the same for all iterations. The initial conditions generated by the SI model for cycle *HCCI0* are stored

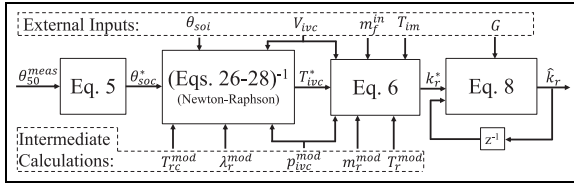


**Figure 8.** Block diagram summary of  $k_r$  parameter update method. All quantities evaluated on cycle  $HCCI 0$  during an SI–HCCI transition.

and used to initialize each trial. Figure 9 plots the  $\hat{k}_r$  parameter dynamics as a function of mode transition iteration for several values of the adaptive gain  $G$ , along with the model's transient  $\theta_{50}$  prediction as  $\hat{k}_r$  adapts for a fixed  $G = 0.1$  in the bottom subplot. The left column shows the perfect case where each iteration of the mode transition yields exactly the same  $\theta_{50}$  on cycle  $HCCI 0$ , which is the reason for the constant line in the middle subplot. In the right column, zero-mean Gaussian white noise with a standard deviation of 2 CAD is added to the base  $\theta_{50}$  from the perfect case to emulate the effect of process and measurement noise altering the measured  $\theta_{50}$  on each iteration of the mode transition sequence.

Starting from the initialized value of  $\hat{k}_r$  in Figure 9, the model  $\theta_{50}$  prediction has large errors both on cycle  $HCCI 0$  and the following HCCI cycles. As consecutive iterations are carried out, the  $\hat{k}_r$  estimate increases, resulting in a significant improvement in the model's  $\theta_{50}$  prediction. The value to which  $\hat{k}_r$  converges is the same for both the clean and noisy  $\theta_{50}$  measurement cases, although close comparison of the right and left columns of Figure 9 shows that convergence speed can be slightly inhibited by the presence of noise. This indicates that the adaptation may be hindered to a minor extent in the presence of noise, but it is still able to converge robustly. The lines of multiple  $G$  values show how the adaptation can be sped up by increasing the gain, at the cost of increased noise amplification. Experimental tuning of the gain in further mode transition testing is necessary to definitively balance this trade-off.

Another concern with the  $k_r$  adaptation is the effect of modeling error on the convergence of the algorithm. To examine a scenario where the model parameters are perturbed from the nominal case, a 5% error is introduced into two uncertain quantities which affect the in-cylinder the temperature and hence the  $k_r$  adaptation: the model's prediction of residual mass  $m_r$ , and the initial condition for the exhaust temperature on cycle  $HCCI 0$  that is carried over from SI, denoted  $T_{bd}$  ( $HCCI 0$ ). The parameter adaptation is rerun starting from the same condition as in Figure 9, using a constant  $G = 0.1$  with no noise for simplicity. The results are plotted in Figure 10, where the left column considers the  $m_r$  perturbation and the right column considers the  $T_{bd}$  ( $HCCI 0$ ) perturbation. As can be seen, for both positive and negative 5% error in these quantities,

the adaptation adjusts the  $\hat{k}_r$  so that the  $\theta_{50}$  is matched on cycle  $HCCI 0$ . The final value to which the parameter converges varies from the nominal case depending on the perturbation, as is necessary to match  $\theta_{50}$  on cycle  $HCCI 0$  when the perturbation is applied. The model  $\theta_{50}$  prediction as shown in the middle and bottom subplots improves with increasing adaptive iterations; however, in the case of  $-5\%$  error in  $m_r$ , the model  $\theta_{50}$  predictions on the cycles following cycle  $HCCI 0$  still have large error after many iterations. This is because the combustion phasing on cycle  $HCCI 1$  is very late and near a misfire condition, where the Arrhenius integral for combustion phasing becomes very sensitive, and so the  $-5\%$  error in  $m_r$  can result in large errors in combustion phasing for the model. In controller implementation, the controller will be tuned to avoid these near-misfire conditions so that the model predictions do not become so sensitive.

### Model evaluation in multiple SI–HCCI transition conditions

To examine the ability of the proposed model and residual temperature correction method to extend to various mode transition conditions, several additional SI–HCCI transition experiments were carried out for comparison of the model predictions versus data. These experiments differ from the previously presented mode transition in that the intake cam is switched to low-lift prior to the exhaust cam so that the SI phase of the transition operates with a low-lift intake cam, and the point of entry to HCCI is defined solely by the switch of the exhaust cam to low lift. This approach has some minor advantages and disadvantages to switching both the intake and exhaust cams at the same time as in the mode transition in Figure 5; however, experimentation indicates that for a wide range of intake cam phasings, the switch of the intake cam from high to low lift has negligible effect on the air-path and combustion. The effects are predominantly driven by the exhaust cam switch and associated increase in internal residual. In any case, the ability of the model to predict the combustion outputs in both Figure 5 and the mode transitions of this section corroborates that it can be used with either intake switching strategy.

As stated earlier during the discussion of adaptive parameter tuning, when multiple SI–HCCI transition conditions are considered, the value of the residual temperature correction  $k_r$  to match transient data will most likely vary with operating condition. Hence, the model accuracy can be improved by introducing a dependency of  $k_r$  on the engine operating variables, as opposed to the constant value in earlier sections where a single-mode transition case was considered. A simple linear parameterization of  $k_r$  to the EVC timing on cycle  $HCCI 0$  provided adequate model accuracy for a dataset of multiple mode transition trials at 2000 r/min

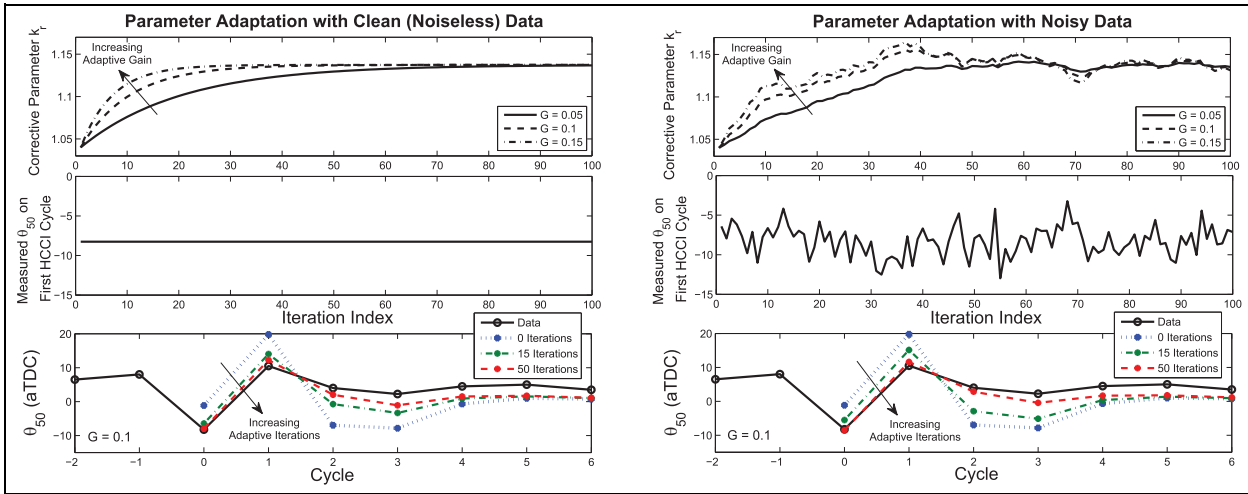


**Figure 9.** Demonstration of  $k_r$  adaptation for the SI–HCCI mode transition sequence of Figure 5 with perfect repeatability (left) and additive noise (right) in the  $\theta_{50}$  measurement that is assimilated on cycle HCCI 0. Top: adaptive parameter dynamics as a function of mode transition iteration; middle:  $\theta_{50}$  value on cycle HCCI 0 that is fed to the adaptation after being corrupted by ensemble noise; bottom: refinement in model  $\theta_{50}$  response as  $\hat{k}_r$  adapts for fixed  $G = 0.1$ .

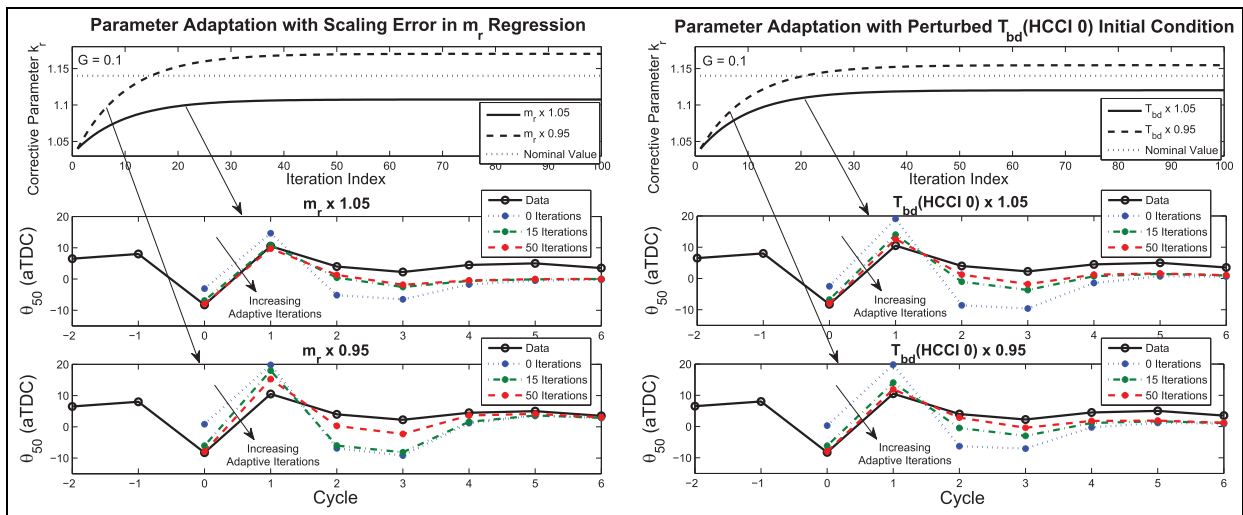


**Figure 10.** Demonstration of  $k_r$  adaptation for the SI–HCCI mode transition sequence of Figure 5 in the presence of perturbations to the modeled  $m_r$  and  $T_{bd}$  (HCCI 0). Top: adaptive parameter dynamics with consecutive mode transition iterations; middle/bottom: model reproduction of measured  $\theta_{50}$  response from the mode transition with varying amounts of adaptive iteration for  $\pm 5\%$  model perturbation.

engine speed which includes those presented in this section

$$k_r \approx a_1 \theta_{evc}^{HCCI0} + a_0 \quad (9)$$

The logic behind this choice of  $k_r$  parameterization is that the EVC timing when switching to HCCI presents significant uncertainty to the nominal model because it tends to be later than any setting that can be reached in steady-state HCCI for a given fuel injection quantity/timing due to the high exhaust temperature carried over from SI. The linear form of the parameterization maintains compatibility with the adaptive tuning method of section “Adaptive tuning of augmented parameter,” although now the adaptive gain  $G$  will vary based on

the measured quantities according to the chosen parameter update law.

One aspect that was explored with additional mode transition experiments was the ability of the model to capture the output response when the initial conditions for switching to HCCI are changed, while keeping the operating condition similar to that in Figure 5. The initial conditions are altered through adjusting several different input commands to the final SI cycle. Figure 11 plots the most important inputs and modeled versus measured outputs for several different methods of perturbing the HCCI initial conditions. In the left column, the time at which the throttle is commanded open to switch to HCCI is delayed so that the intake pressure is

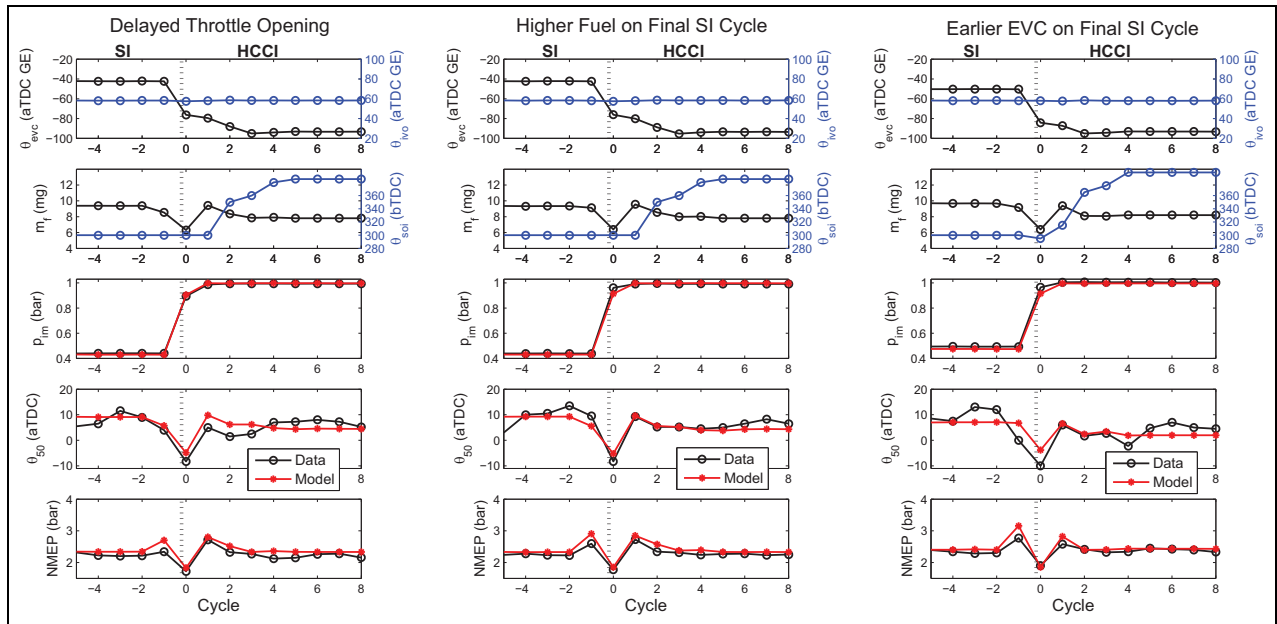


**Figure 11.** Experimental SI–HCCI mode transitions at low load HCCI with varying initial conditions for the HCCI phase of the transition. Left: delayed throttle opening when switching to HCCI; middle: higher fuel quantity on final SI cycle; right: earlier EVC timing when switching to HCCI.

lower on cycle *HCCI 0*. In the center column, the fuel injected into cycle *SI -1* is increased relative to the nominal fuel sequence, increasing the exhaust temperature of the residual gas passed to cycle *HCCI 0*. In the right column, the *SI* switch point is set with an earlier exhaust valve timing to increase the trapped residual mass leading to cycle *HCCI 0*. Throughout these various perturbations to the HCCI initial condition, the model reproduces the general trend of the output time histories well, with quantitative accuracy that is acceptable for control purposes. Note that the somewhat non-obvious reason for the increase in NMEP on cycle *SI -1* is the exhaust cam switch to low lift, which shifts the EVO timing later and elongates the expansion stroke, increasing the work output. The effect is more dramatic at the earlier exhaust valve timings present in the low load mode transitions of Figure 11. It will be seen in the next set of experiments with higher load trials that the effect is mitigated at later exhaust valve timings.

Another set of SI–HCCI mode transition experiments were concerned with evaluating the model’s performance in varying operating conditions. The operating condition is adjusted by sweeping the load from near the lower HCCI limit to near the upper HCCI limit for the experimental engine at 2000 r/min. The engine speed is not changed because the model parameterization did not contain speed variation. The results for three of these experiments are presented in Figure 12, starting near the lower load limit in the left column and increasing to the high load limit in the right column. As the load condition varies, the actuator sequences for the EVC timing and the fuel injection quantity/timing vary as well, which adds diversity to

the dataset. Throughout the multiple actuator sequences, again the model is able to reproduce the output time histories well, with the only problem occurring with the NMEP prediction on cycle *HCCI 1* of the low load sequence. The model’s overestimation of the NMEP on this cycle can be explained by the late combustion phasing present in the data, where the roll-off of combustion efficiency with combustion phasing becomes steep<sup>33</sup> and so even a few degrees of  $\theta_{50}$  error can make a large difference in the NMEP prediction. The model-predicted  $\theta_{50}$  is several degrees earlier than the data value on this cycle, and so the model does not register the reduced torque from the late phasing. As was earlier noted when a similar phenomenon arose in Fig. 10, in implementation the controller will be tuned to avoid these late phasing points so that the model predictions do not become so sensitive. A last note is that the NMEP rise on cycle *SI -1* of the low load case is less pronounced than in the mode transition in the left column of Figure 11 despite similar actuator settings, which may be due to deviation of the injected fuel quantity from the commanded value or other stochastic disturbances.

## Conclusion

A low-order MVEM for model-based control of SI–HCCI mode transitions has been presented. The model includes discrete SI and HCCI combustion modes that are linked through exhaust gas temperature and composition states and a continuous time air-path which is based on 0-D manifold filling dynamics. The combustion models were parameterized to a wide range of



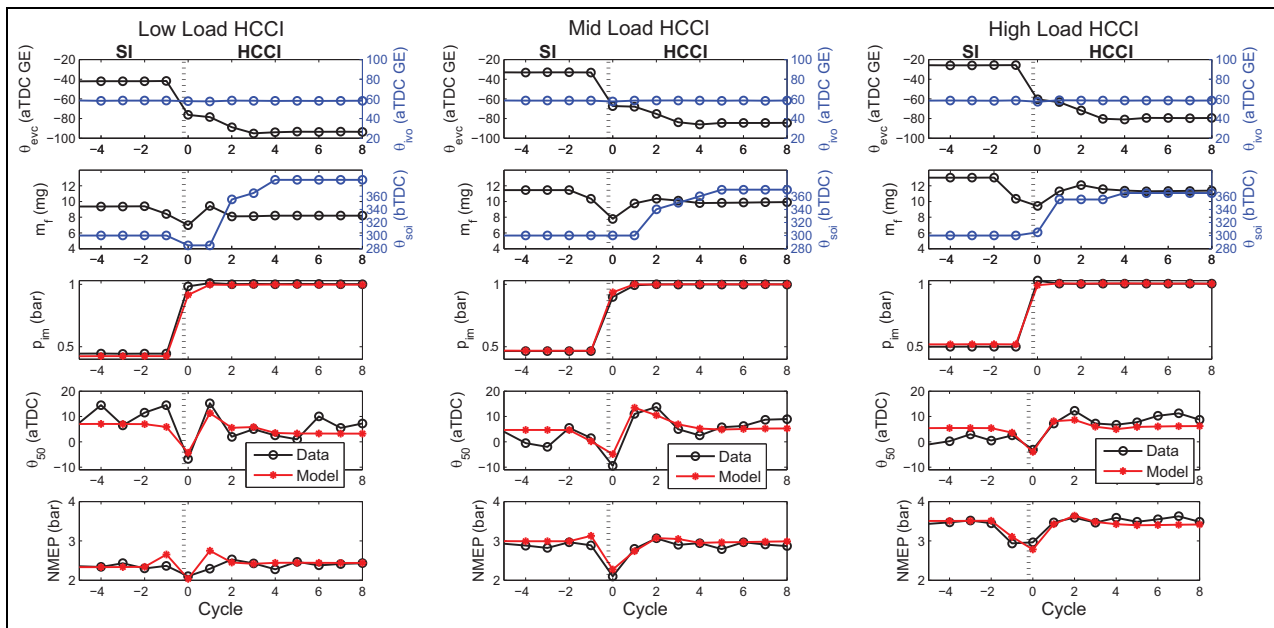


**Figure 12.** Experimental SI–HCCI mode transitions across the HCCI load range at 2000 r/min. Left: low load; middle: mid load; right: high load.

steady-state data, most notably with the HCCI model being exposed to throttled operation and a wide range of AFR variation in preparation for possible entry to these conditions during cam switching SI–HCCI transitions with two-stage cam hardware. Despite the adequate steady-state fit, the model produced significant errors when simulated with SI–HCCI mode transition data, which were traced to the first HCCI cycle of the transition where the conditions can be significantly outside any that can be accessed in steady-state data used to parameterize the model. A correction factor for residual gas temperature motivated by the high exhaust temperature that is carried over from SI leading into the first HCCI cycle was introduced to account for the model error, after which the model predicted transient SI–HCCI combustion phasing and torque output time histories well. Using a simple parameterization for the residual temperature correction as a linear function of EVC timing, the model was shown to capture multiple SI–HCCI transition experiments involving varying initial conditions for the HCCI combustion and varying load conditions over the HCCI load range. A routine to update the residual temperature correction factor using online SI–HCCI transition data was proposed, in order to make use of feedback for control of the first transient HCCI cycle and to improve the model predictions where steady-state parameterization data were not available. The online adaptation was shown to significantly improve the model predictions when conditioned on consecutive SI–HCCI transition trials and converged robustly in the presence of noise and model perturbations.

Experimental testing and potential modification of the modeling methodology for the HCCI–SI direction of the mode transition are open topics for future work. Additionally, extension of the low-order HCCI

modeling approach of this article to encompass the effects of spark assist is a pertinent topic for future research, as many mode transition studies<sup>5,6,8,10,12</sup> have found spark assist to be helpful.

### Acknowledgements

This work was performed as a part of the ACCESS project consortium (Robert Bosch LLC, AVL Inc., Emitec Inc., Stanford University, University of Michigan) under the direction of PI Hakan Yilmaz and Co-PI Oliver Miersch-Wiemers, Robert Bosch LLC.

### Declaration of conflicting interests

The author declares no potential conflicts of interest with respect to the research, authorship, and/or publication of this article.

### Disclaimer

This report was prepared as an account of work sponsored by an agency of the US Government. Neither the US Government nor any agency thereof, nor any of their employees, makes any warranty, express or implied, or assumes any legal liability or responsibility for the accuracy, completeness, or usefulness of any information, apparatus, product, or process disclosed, or represents that its use would not infringe privately owned rights. Reference herein to any specific commercial product, process, or service by trade name, trademark, manufacturer, or otherwise does not necessarily constitute or imply its endorsement, recommendation, or favoring by the US Government or any agency thereof. The views and opinions of authors expressed herein do not necessarily state or reflect those of the US Government or any agency thereof.

## Funding

The author(s) disclosed receipt of the following financial support for the research, authorship, and/or publication of this article: This material was based on the work supported by the Department of Energy (National Energy Technology Laboratory) under Award number DE-EE0003533.

## References

- Zhao F, Asmus T, Assanis D, Dec J, Eng J and Najt P. *Homogeneous Charge Compression Ignition (HCCI) engines: key research and development issues*. Warrendale, PA: SAE International, 2003.
- Dec J and Yang Y. Boosted HCCI for high power without engine knock and with ultra-low NO<sub>x</sub> emissions—using conventional gasoline. *SAE Int J Engine* 2010; 3(1): 750–767.
- Koopmans L, Ström H, Lundgren S, Backlund O and Denbratt I. Demonstrating a SI-HCCI-SI mode change on a Volvo 5-cylinder electronic valve control engine. SAE technical paper 2003-01-0753, 2003.
- Santoso H, Matthews J and Cheng W. Managing SI/HCCI dual-mode engine operation. SAE technical paper 2005-01-0162, 2005.
- Zhang Y, Xie H, Zhou N, Chen T and Zhao H. Study of SI-HCCI-SI transition on a port fuel injection engine equipped with 4VVAS. SAE technical paper 2007-01-0199, 2007.
- Milovanovic N, Blundell D, Gedge S and Turner J. SI-HCCI-SI mode transition at different engine operating conditions. SAE technical paper 2005-01-0156, 2005.
- Tian G, Wang Z, Ge Q, Wang J and Shuai S. Control of a spark ignition homogeneous charge compression ignition mode transition on a gasoline direct injection engine. *Proc IMechE, Part D: J Automobile Engineering* 2007; 221: 867–875.
- Cairns A and Blaxill H. The effects of two-stage cam profile switching and external EGR on SI-CAI combustion transitions. SAE technical paper 2007-01-0187, 2007.
- Kalian N, Zhao H and Qiao J. Investigation of transition between spark ignition and controlled auto-ignition combustion in a V6 direct-injection engine with cam profile switching. *Proc IMechE, Part D: J Automobile Engineering* 2008; 222: 1911–1926.
- Wu H, Collings N, Regitz S, Etheridge J and Kraft M. Experimental investigation of a control method for SI-HCCI-SI transition in a multi-cylinder gasoline engine. SAE technical paper 2010-01-1245, 2010.
- Nier T, Kulzer A and Karrelmeyer R. Analysis of the combustion mode switch between SI and gasoline HCCI. SAE technical paper 2012-01-1105, 2012.
- Kakuya H, Yamaoka S, Kumano K and Sato S. Investigation of a SI-HCCI combustion switching control method in a multi-cylinder gasoline engine. SAE technical paper 2008-01-0792, 2008.
- Gorzelic P, Hellström E, Stefanopoulou A and Jiang L. Model-based feedback control for an automated transfer out of SI operation during SI to HCCI transitions in gasoline engines. In: *ASME dynamic systems and control conference*, Fort Lauderdale, FL, 17–19 October 2012, pp.359–367. New York: ASME.
- Ravi N, Jagsch M, Oudart J, Chaturvedi N, Cook D and Kojic A. Closed-loop control of SI-HCCI mode switch using fuel injection timing. In: *ASME dynamic systems and control conference*, Palo Alto, CA, 21–23 October 2013, pp.V001T12A001. New York: ASME.
- Roelle M, Shaver G and Gerdes J. Tackling the transition: a multi-mode combustion model of SI and HCCI for mode transition control. In: *ASME international mechanical engineering congress and exposition*, Anaheim, CA, 13–19 November 2004, pp.329–336. New York: ASME.
- Shaver G, Roelle M and Gerdes J. Modeling cycle-to-cycle dynamics and mode transition in HCCI engines with variable valve actuation. *Control Eng Pract* 2006; 14: 213–222.
- Yang X, Zhu G and Sun Z. A control oriented SI and HCCI hybrid combustion model for internal combustion engines. In: *ASME dynamic systems and control conference*, Cambridge, MA, 12–15 September 2010, pp.657–664. New York: ASME.
- Yang X and Zhu G. A two-zone control oriented SI-HCCI hybrid combustion model for the HIL engine simulation. In: *IEEE American control conference*, San Francisco, CA, 29 June–1 July 2011, pp.973–978. New York: IEEE.
- Ravi N, Roelle M, Liao H, Jungkunz A, Chang C, Park S, et al. Model-based control of HCCI engines using exhaust recompression. *IEEE T Contr Syst T* 2010; 18(6): 1289–1302.
- Jiang L, Stefanopoulou A, Vanier J and Yilmaz H. Parameterization and simulation for a turbocharged spark ignition direct injection engine with variable valve timing. SAE technical paper 2009-01-0680, 2009.
- Lee D, Jiang L, Yilmaz H and Stefanopoulou AG. Air charge control for turbocharged spark ignition engines with internal exhaust gas recirculation. In: *IEEE American control conference*, Baltimore, MD, 30 June–2 July 2010, pp.1471–1476. New York: IEEE.
- Gorzelic P, Hellström E, Stefanopoulou A, Jiang L and Gopinath S. A coordinated approach for throttle and wastegate control in turbocharged spark ignition engines. In: *IEEE Chinese control and decision conference*, Taiyuan, China, 23–25 May 2012, pp.1524–1529. New York: IEEE.
- Eriksson L. Modeling and control of turbocharged SI and DI engines. *Oil Gas Sci Technol* 2007; 62(4): 523–538.
- P. Gorzelic. *Modeling and Model-Based Control of Multi-Mode Combustion Engines for Closed-Loop SI/HCCI Mode Transitions with Cam Switching Strategies*. Ph.D. Thesis, University of Michigan-Ann Arbor, USA, 2015.
- Jade S, Hellström E, Larimore J, Stefanopoulou A and Jiang L. Reference governor for load control in a multi-cylinder recompression HCCI engine. *IEEE T Contr Syst T* 2014; 22(4): 1408–1421.
- Ravi N, Liao HH, Jungkunz A, Chang CF, Song H and Gerdes J. Modeling and control of an exhaust recompression HCCI engine using split injection. *J Dyn Syst: T ASME* 2012; 134: 231–250.

27. Song HH and Edwards CF. Understanding chemical effects in low-load-limit extension of homogeneous charge compression ignition engines via recompression reaction. *Int J Engine Res* 2009; 10: 231–250.
28. Yun H, Guralp O, Grover R and Najt P. The effect of temperature and oxygen concentration on auto-ignition at low-load operating conditions in a gasoline homogeneous charge compression ignition engine. *Int J Engine Res* 2013; 14(5): 512–524.
29. He X, Donovan M, Zigler B, Palmer T, Walton S, Woolridge M, et al. An experimental and modeling study of iso-octane ignition delay times under homogeneous charge compression ignition conditions. *Combust Flame* 2005; 142: 266–275.
30. Shaver G, Gerdes J, Roelle M, Caton P and Edwards C. Dynamic modeling of residual-affected homogeneous charge compression ignition engines with variable valve actuation. *J Dyn Syst: T ASME* 2005; 127(3): 374–381.
31. Hellström E and Stefanopoulou A. Modeling cyclic dispersion in autoignition combustion. In: *IEEE conference on decision and control*, Orlando, FL, 12–15 December 2011, pp.6834–6839. New York: IEEE.
32. Jankovic M and Magner S. Variable cam timing: consequences to automotive engine control design. In: *IFAC triennial world conference*, 2002. Barcelona, Spain. Spain: International Federation of Automatic Control.
33. Eriksson L and Andersson I. An analytic model for cylinder pressure in a four stroke SI engine. SAE technical paper 2002-01-0371, 2002.
34. Hellström E, Stefanopoulou A, Vavra J, Babajimopoulos A, Assanis D, Jiang L, et al. Understanding the dynamic evolution of cyclic variability at the operating limits of HCCI engines with negative valve overlap. *SAE Int J Engine* 2012; 5(3): 995–1008.
35. Gorzelic P, Shingne P, Martz J, Stefanopoulou A, Sterniak J and Jiang L. A low-order HCCI model extended to capture SI-HCCI mode transition data with two-stage cam switching. In: *ASME dynamic systems and control conference*, San Antonio, TX, 22–24 October 2014, pp.V002T34A005. New York: ASME.
36. Nuësch S, Hellström E, Jiang L and Stefanopoulou A. Influence of transitions between SI and HCCI combustion on driving cycle fuel consumption. In: *European control conference*, Zürich, 17–19 July 2013, pp.1976–1981. New York: IEEE.
37. Astrom K and Wittenmark B. *Adaptive control*. Addison-Wesley, 1995, New York.

## Appendix I

### HCCI model equations

Arbitrary  $a_i$  represents fitting coefficients. Superscript 0 indicates a delayed value from the previous cycle. The cylinder volume at any event  $e$  is found with the crank-slider equation and designated by  $V_e$ .

Cycle delayed states:

$$x = [T_{bd}^0 \quad b_{bd}^0 \quad f_{bd}^0] \quad (10)$$

Residual gas mass (inspired by ideal gas law at exhaust valve closing (EVC))

$$m_r = \frac{(a_1 \theta_{evc} + a_2) V_{evc}}{R(a_3 T_{bd}^0 + a_4)} \quad (11)$$

Residual air mass:

$$m_{ra} = m_r(1 - b_{bd}^0 - f_{bd}^0) \quad (12)$$

Temperature at EVC (prior to recompression heat release (RCHR))

$$T_{evc} = a_1 T_{bd}^0 + a_0 \quad (13)$$

RCHR: Here,  $\mu > 0$  is a tuning factor representing heat losses and idealities of instantaneous combustion,  $m_{rf}^b$  is the mass of residual fuel that burns in recompression, and  $c_v$  is the fixed constant volume specific heat. Equation (16) is necessary to account for rich/slightly lean scenarios wherein there is not enough available air recycled from the previous combustion to combust all the unburnt fuel

$$T_{rc} = T_{evc} + \Delta T_{rc} \quad (14)$$

$$\Delta T_{rc} = \mu \frac{m_{rf}^b Q_{lhv}}{c_v m_r} \quad (15)$$

$$m_{rf}^b = \min[m_r f_{bd}^0, m_{ra}/AFR_s] \quad (16)$$

Implementation note: In parameterization, the tuning factor  $\mu$  is factored into the  $a_m$  parameter vector defined in Appendix 2. This allows the effect of any mild RCHR caused by  $\eta_{50}$  (see equation (38)) falling slightly below unity at later combustion phasings in steady-state data to be accounted for. Because the effect of RCHR is difficult to observe from cycle-averaged steady-state data, the parameter regression tends to drive  $\mu$  to near-zero values, and so  $\mu$  must be lower bounded for RCHR to be seen in transient. A lower bound of 0.4 was chosen here.

Total fuel mass:

$$m_f = m_f^{in} + (m_r f_{bd}^0 - m_{rf}^b) \quad (17)$$

Recompression relative AFR

$$\lambda_r = \frac{m_{ra}}{AFR_s m_f} \quad (18)$$

Residual gas temperature:

$$T_r = a_1 T_{rc} + a_2 \lambda_r \theta_{soi} + a_3 \quad (19)$$

Pressure at IVC:

$$p_{ivc} = a_1 p_{im} + a_0 \quad (20)$$

Mass of inducted air (see equation (4)): This equation comes from substituting the ideal gas law for  $m_c$  into an energy balance at IVC, upon which  $T_{ivc}$  cancels and the mass of fresh air  $m_a$  can be isolated. The coefficients  $a_1$  and  $a_2$  are introduced to improve the fit to data.

Total mass of air:

$$m_a^{tot} = m_a^{in} + m_{ra} \quad (21)$$

Total cylinder mass:

$$m_c = m_r + m_a + m_f^{in} \quad (22)$$

Burned gas fraction before combustion

$$b_c = \frac{m_c - m_a^{tot} - m_f}{m_c} \quad (23)$$

Temperature at IVC

$$T_{ivc} = \frac{p_{ivc} V_{ivc}}{R m_c} \quad (24)$$

AFR

$$\lambda_{ex} = \frac{m_a^{in}}{m_f AFR_s} \quad (25)$$

$$\lambda_c = \frac{m_a^{tot}}{m_f AFR_s} \quad (26)$$

Arrhenius integral for start of combustion

$$K_{th}(\theta_{soi}, \lambda_r, T_{rc}) = \int_{\theta_{ivc}}^{\theta_{soc}} \frac{1}{\omega} p_c(\theta)^{n_p} e^{\left(\frac{-E_a}{RT_c(\theta)}\right)} d\theta \quad (27)$$

$$K_{th}(\theta_{soi}, \lambda_r, T_{rc}) = (a_{12}\lambda_r^2 + a_{11}\lambda_r + a_{10})\theta_{soi} + a_{02}\lambda_r^2 + a_{01}\lambda_r + a_{00} + (a_{T1}\lambda_r\theta_{soi} + a_{T0})T_{rc} \quad (28)$$

$$p_c(\theta) = p_{ivc} \left(\frac{V_{ivc}}{V(\theta)}\right)^{n_c}, \quad T_c(\theta) = T_{ivc} \left(\frac{V_{ivc}}{V(\theta)}\right)^{n_c-1} \quad (29)$$

Implementation note:  $\lambda_r$  is allowed to take negative values in equation (28) to capture the trend with rich combustion. A negative  $\lambda_r$  is necessary to detect rich combustion from the previous cycle because the simple composition dynamics (12) and (45) impose that  $m_{ra}$  takes a negative value when the total air mass is less than the stoichiometric amount.  $m_{ra}$  is saturated at 0 when used in equation (21), however, to retain physicality. Also, to prevent extreme sensitivity to  $\lambda_r$  as the quadratic dependence in equation (28) is extrapolated to high  $\lambda_r$  values outside the parameterized range,  $\lambda_r$  is modified by a hyper tangent function which forces  $\lambda_r$  to roll-off as it exceeds a value significantly beyond the parameterized range

$$\tilde{\lambda}_r = a_{sat}\lambda_r^{max} \tanh\left(\frac{\lambda_r}{a_{sat}\lambda_r^{max}}\right) \quad (30)$$

$\lambda_r^{max}$  is let to vary as a linear function of  $\theta_{soi}$  which upper bounds the maximum  $\lambda_r$  values in the data, as typically earlier  $\theta_{soi}$  timings allow higher  $\lambda_r$  values to be reached without risk of misfire.  $a_{sat}$  specifies how far past  $\lambda_r^{max}$  that the  $\lambda_r$  value in equation (28) ultimately becomes saturated.

Crank angle at 50% mass fraction burned

$$\theta_{50} = a_1\theta_{soc} + a_0 \quad (31)$$

Volume at instantaneous combustion

$$V_{comb} = V(|\theta_{50} - \theta_{50}^{MBT}|) = V(|\theta_{50} - 5|) \quad (32)$$

Pressure and temperature before combustion (polytropic exponents determined through torque regression)

$$p_{bc} = p_{ivc} \left(\frac{V_{ivc}}{V_{comb}}\right)^{n_c} \quad (33)$$

$$T_{bc} = T_{ivc} \left(\frac{V_{ivc}}{V_{comb}}\right)^{n_c-1} \quad (34)$$

Pressure and temperature after combustion

$$p_{ac} = p_{bc} \left(\frac{T_{ac}}{T_{bc}}\right) \quad (35)$$

$$T_{ac} = T_{bc} + \eta_\lambda \eta_{50} \frac{m_f Q_{lhv}}{c_v m_c} \quad (36)$$

AFR-combined thermal and combustion efficiency

$$\eta_\lambda = \frac{a_1 \lambda_c + a_2}{\lambda_c + a_3} \quad (37)$$

Late phasing combustion efficiency:

$$\eta_{50} = \frac{a_1}{1 + \exp\left(\frac{\theta_{50} - \theta_{50}^*(m_f)}{a_2}\right)} \quad (38)$$

$$\theta_{50}^*(m_f) = a_3 m_f + a_4 \quad (39)$$

Implementation note: It is ideal to tune the coefficients  $a_1$ – $a_4$  with post-processed combustion efficiency estimates from high cyclic variability data as in Hellström and Stefanopoulou;<sup>30</sup> however, such data were not available for this study. Instead, the coefficients were manually tuned to position the roll-off of the sigmoid near the late phasing limit observed from steady-state data across different loads.

Pressure and temperature at EVO:

$$p_{evo} = p_{ac} \left(\frac{V_{comb}}{V_{evo}}\right)^{n_e} \quad (40)$$

$$T_{evo} = T_{ac} \left(\frac{V_{comb}}{V_{evo}}\right)^{n_e-1} \quad (41)$$

Exhaust blowdown temperature:

$$T_{bd} = T_{evo} \left(\frac{p_{em}}{p_{evo}}\right)^{1-\frac{1}{n_{bd}}} \quad (42)$$

Mass of unburnt fuel:

$$m_{uf} = m_f(1 - \max[(1 - \lambda_c), 0])\eta_{50} \quad (43)$$

Burned gas fraction in the exhaust

$$b_{bd} = \frac{(AFR_s + 1)(m_f - m_{uf})}{m_c} + b_c \quad (44)$$

Unburnt fuel mass fraction in the exhaust

$$f_{bd} = \frac{m_{uf}}{m_c} \quad (45)$$

Cycle work:

$$W_{cig} = \frac{p_{bc} V_{comb} - p_{ivc} V_{ivc}}{1 - n_c} + \frac{p_{evo} V_{evo} - p_{ac} V_{comb}}{1 - n_e} \quad (46)$$

$$IMEP = \frac{W_{cig}}{V_d} \quad (47)$$

$$NMEP = IMEP - PMEP \quad (48)$$

$$PMEP \approx \text{const} \quad (49)$$

## Appendix 2

### HCCI model parameterization

As stated in the model overview, the HCCI model is parameterized in an iterative routine to account for compounding of modeling error through cycle-to-cycle couplings. The parameterization algorithm also includes the option for simulation of the model with transient mode switch data in the iterative loop so that the coefficients that describe the dependency of the transient  $k_r$  parameter on operating condition as in equation (9) can be automatically tuned to match transient data. To depict the routine graphically, define parameter vectors  $a_r$  to contain the parameters for residual mass  $m_r$  (equation (11)),  $a_T$  to contain the parameters for the EVC temperature  $T_{evc}$  (equation (13)),  $a_m$  to contain the parameters for inducted air mass  $m_a^{in}$  (equations (4) and (19)) as well as the RCHR  $\mu$  parameter (equation (15)),  $a_{50}$  to contain the parameters for combustion phasing (equations (27) and (28)), and  $a_r$  to contain the parameters for torque (equation (37)) as well as the polytropic compression and expansion exponents. Note that  $\theta_{50}$  is linked to  $\theta_{soc}$  through the linear function (31) whose coefficients are held fixed in the iteration. Also note that the polytropic compression exponent  $n_c$  in equation (29) is held fixed at 1.32 to avoid excessive cross-coupling between the torque and combustion phasing regressions. Additionally, the matrix  $\Psi^T$  is defined to contain  $N_{run}$  columns of time histories from SI-HCCI mode transition transient data which are  $N_{cyc}$  rows in duration. For the SI-HCCI mode transition dataset used to parameterize  $k_r$  according to equation (9),  $N_{run} = 9$  and  $N_{cyc} = 3$ .

A flow chart of the regression routine is shown in Figure 13, where  $n$  is the iteration index. The routine is initialized with estimates of the model states and individually parameterized regression coefficients from post-processed steady-state data. From here, the routine steps through the model's regressions, fitting each one individually and using the fitted quantities in subsequent regressions to include the effect of compounding modeling error. The regression for the IVC pressure  $p_{ivc}$  in equation (20) is held fixed in the algorithm because  $p_{ivc}$  is regressed solely as a function of the input  $p_{im}$  and

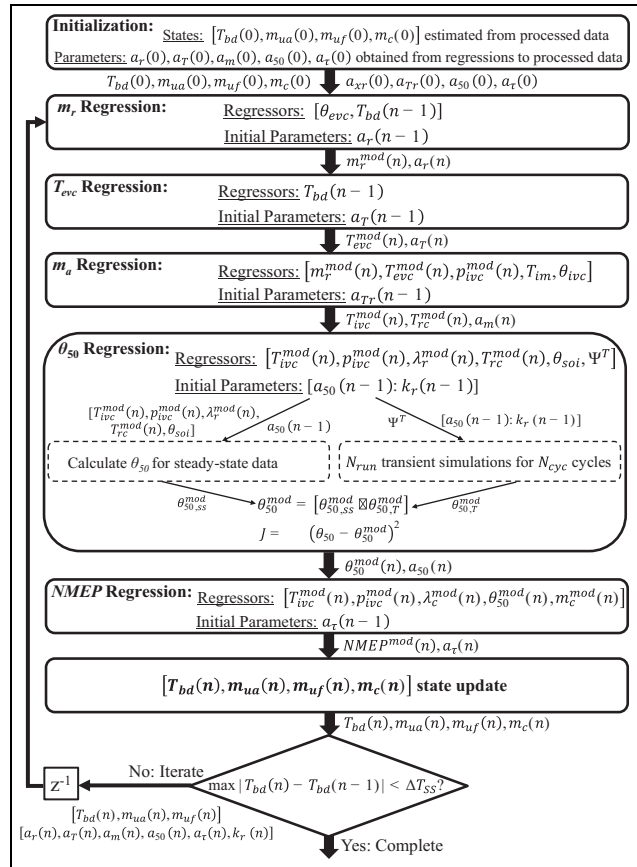


**Figure 13.** Flow chart depicting iterative regression method for both steady-state and transient  $k_r$  model parameters.

so compounding error is not an issue. Note that after the  $T_{evc}$  and  $m_a$  regressions, intermediate variables such as the IVC temperature  $T_{ivc}$  which are not directly regressed are calculated as necessary to generate the full set of regressors for the next regression step. When the  $\theta_{50}$  regression is reached, the  $a_{50}$  coefficients are used to calculate  $\theta_{50}$  for steady-state data  $\theta_{50,ss}^{mod}$  and then concatenated with the  $k_r$  parameter to carry out  $N_{run}$  transient simulations of SI-HCCI mode transitions to produce  $\theta_{50,T}^{mod}$ . The  $\theta_{50,ss}^{mod}$  and  $\theta_{50,T}^{mod}$  vectors are then concatenated into a single vector whose squared error is used to form the cost function for the regression.

At the completion of an iteration, the model states are updated using the calculated variables from the current iteration, and a convergence check is performed on the states. The convergence check adopted here was that the maximum change in the blowdown temperature state from the previous iteration across all steady-state points was less than some threshold  $\Delta T_{SS}$ , chosen to be 1 K. If the convergence check is not met, the states from the current iterate are recycled to the beginning of the model calculations, and the next iteration proceeds using the optimized values from the previous iteration as initial parameter guesses.